

Topological signatures of globular polymers

M. Baiesi,¹ E. Orlandini,^{1,2} A. L. Stella,^{1,2} and F. Zonta¹

¹*Dipartimento di Fisica, Università di Padova, Via Marzolo 8, I-35131 Padova, Italy*

²*Sezione INFN, Università di Padova, Via Marzolo 8, I-35131 Padova, Italy*

(Dated: January 15, 2013)

Simulations in which a globular ring polymer with delocalized knots is separated in two interacting loops by a slipping link, or in two non-interacting globuli by a wall with a hole, show how the minimal crossing number of the knots controls the equilibrium statistics. With slipping link the ring length is divided between the loops according to a simple law, but with unexpectedly large fluctuations. These are suppressed only for unknotted loops, whose length distribution shows always a fast power law decay. We also discover and explain a topological effect interfering with that of surface tension in the globule translocation through a membrane nanopore.

PACS numbers: 36.20.Ey, 02.10.Kn, 87.15.Aa

Most often, ring polymers are experimentally studied in situations in which their topological entanglement does not change in time. However, most of our theoretical and numerical understanding of polymer statistics relies on ensemble descriptions in which the rings assume all possible topologies [1]. An open challenge is that of determining up to what extent specific permanent entanglements in the form of knots or links [2] can affect thermodynamic quantities and what is their possible role in determining peculiar behaviors when the polymer is subject to geometrical constraints interfering with the topology.

Different topologies are expected to determine different non-extensive corrections to the free energy of a single ring in the limit of infinitely long chain. For example, the prime knot components of ring polymers in good solvent are weakly localized in this limit [3, 4]. As a consequence, if N is the chain length, each component determines a correction $\sim k_B \ln(N)/N$ to the entropy per monomer [5, 6]. Indeed, each component behaves asymptotically as a point-like decoration which can place itself anywhere along the ring. Radically different conditions are realized below the theta temperature T_θ [7]. Indeed, in the globular phase knots are expected to delocalize. Numerical simulations indicate that the topological entanglement spreads on average on a portion of the ring whose length is proportional to N [8, 9]. Fixed topology is also known to determine a finite size correction to the free energy of a globular ring, which is asymptotically negligible in comparison with that due to surface tension ($\sim N^{-1/3}$). Indeed, at a temperature $T \approx \frac{2}{3}T_\theta$, the correction per monomer has been estimated [10] as $\sim C n_c^a N^{-2}$ where $a \simeq 1.45$, n_c is the minimal number of crossings of the knot [2], and C is a remarkably large negative amplitude. Thus, n_c qualifies as a topological invariant possibly relevant for the thermodynamics of a globular ring.

In the present work we face the challenge of elucidating the role of this invariant, by establishing some empirical laws through which it rules the statistics of the globule when suitable local geometrical constraints are imposed.

These laws, which generally hold in the presence of remarkably large fluctuations, give a precise meaning to the notion of knot delocalization. We also discover novel thermodynamic phenomena which are a peculiar consequence of topology.

Suppose one forces a ring polymer to pass into a slipping link which divides it into two loops. The link is narrow enough to prevent the passage of topological entanglement from one loop to the other. For instance, if the ring has a composite knot with two prime trefoil (3_1) components [2], things can be arranged so that each fluctuating loop encloses one trefoil knot. The loops are kept unlinked. We model flexible ring configurations as N -step self avoiding polygons on cubic lattice [11]. An attractive interaction J between nearest neighbor visited sites allows to obtain a collapsed globular phase for low enough temperature T [7] (Fig. 1). A Monte Carlo simulation method adequate to preserve the ring topology is the grand-canonical BFACF one [11]. However, straightforward application of BFACF to the globule meets a difficulty. Indeed, indicating by K the step fugacity and by Z_N the canonical partition function, the grand canonical average $\langle N \rangle = \Sigma_N N K^N Z_N / \Sigma_N K^N Z_N$ does not grow continuously to $+\infty$ upon approaching from below the critical value K_c of the fugacity. To the contrary, one gets evidence of a discontinuous infinite jump right at $K = K_c$ [8]. We understand here this behavior in the light of the expected [10, 12] asymptotic form of Z_N :

$$\ln(Z_N) = -F_N/kT \sim \text{const} + \mu N + \sigma N^{2/3} + (\alpha - 2) \ln(N) + \frac{C n_c^a}{N} \quad (1)$$

where $\mu = -\ln(K_c)$, $\sigma < 0$ is the interfacial tension, and α is an unknown specific heat exponent that is expected to be independent of topology. The last term on the r.h.s. of Eq.(2) is the above mentioned topological correction to the total free energy F_N . The presence of the surface term $\sim \sigma N^{2/3}$ implies that $\langle N \rangle$ can not diverge continuously to $+\infty$ for K approaching K_c from below. In order to allow a continuous growth of $\langle N \rangle$,

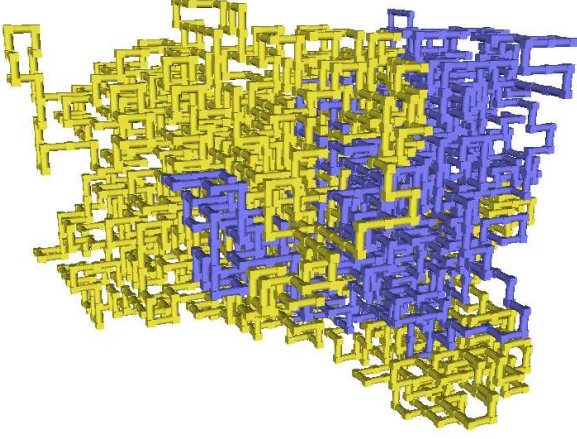


FIG. 1: $N = 2040$ globule with slip link separating a 3_1 knot in loop 1 (yellow) from a 4_1 knot in loop 2 (blue).

we choose to multiply the usual grand-canonical weight of the ring configurations by a factor $\exp[(N - N_0)^2/v]$ which forces N itself to fluctuate around a value close to N_0 if v is chosen small enough. Using still BFACF moves the simulation augmented with the new statistical weight allows a quasi-canonical sampling of configurations with N close to the value determined also by N_0 and v . To improve sampling efficiency, we also implement a multiple Markov chain scheme [13] over different values of N_0 keeping K fixed. Nevertheless, the simulations need a long CPU time (months) to sample a consistent statistics. For this reason we choose to sample only at the temperature $T = 2.5J$, as in [10].

Extensive simulations of the 3_1 vs 3_1 configuration allow to sample for various restricted ranges of N the probability density function (PDF) of l_1/N , $P(l_1/N)$, where l_1 is the fluctuating length of one of the loops (Fig. 2a). Remarkably, even for large N the histogram does not seem to present the bimodal shape found in the good solvent case and indicating a dominance of configurations with large unbalance between l_1 and l_2 [3, 8]. To the contrary, an asymptotically flat histogram seems compatible with the data. Thus, while the two loops on average share equally the total ring length (Fig. 2b), there are very broad fluctuations because all possible partitions of the total ring length are almost equally probable.

To gain further insight, we simulate also the case in which the loops are both unknotted. In this case strongly unbalanced situations are clearly favoured. The PDF of the length of the smaller loop, say l_1 , shows a power law decay $\sim l_1^{-x}$, with $x = 1.55 \pm 0.04$ (Fig. 3). This suggests that the metric exponent of this loop is $\nu = x/d \approx 0.52$. A value of ν close to $1/2$ is consistent with the expectation of Gaussianity of a collapsed chain on relatively small length scales [14]. When for example only loop 2 has a 3_1 knot, while loop 1 is unknotted (\emptyset), we observe that l_1 never grows substantially compared to N ,

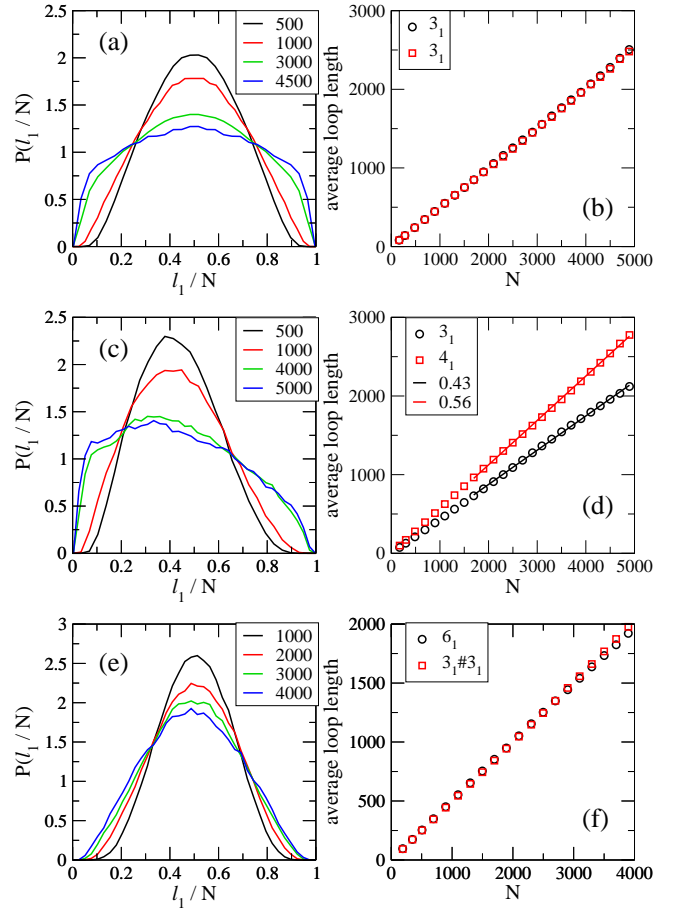


FIG. 2: (a) Histograms of $P(l_1/N)$ for 3_1 vs 3_1 . Different curves correspond to different N values (see legend). (b) $\langle l_1 \rangle_N$ (circles) and $\langle l_2 \rangle_N$ (squares) as a function of N . (c) Histograms of $P(l_1/N)$ for 3_1 vs 4_1 and (d) corresponding average loop lengths. (e) Histograms of $P(l_1/N)$ for 6_1 (loop 1) vs $3_1 \# 3_1$ and (f) corresponding average loop lengths.

and the same power law behavior holds for the PDF of l_1 (Fig. 3). This power-law, implying that $\langle l_1 \rangle \sim N^{0.45(4)}$, denotes a weak localization of the unknotted loop.

The above results are fully consistent with delocalization of the 3_1 knot inside the ring, since in no case a loop containing the knot displays a stable regime in which its average length is a vanishing fraction of N . Similar results hold if 3_1 is replaced by another prime knot. We further examine a competition 3_1 vs 4_1 . The plots reported in Fig. 2c show that also in this case the lengths of the loops keep fluctuating very broadly for increasing N , while $P(l_1/N)$ is not symmetric with respect to $l_1/N = 1/2$ anymore. Quite remarkably, in this and similar competitions (3_1 vs 7_1 , 4_1 vs 6_1 etc.), a simple law is well obeyed by the canonical averages $\langle l_1 \rangle_N$ and $\langle l_2 \rangle_N$:

$$\langle l_i \rangle_N = N \frac{n_{ci}}{n_{c1} + n_{c2}}, \quad i = 1, 2. \quad (2)$$

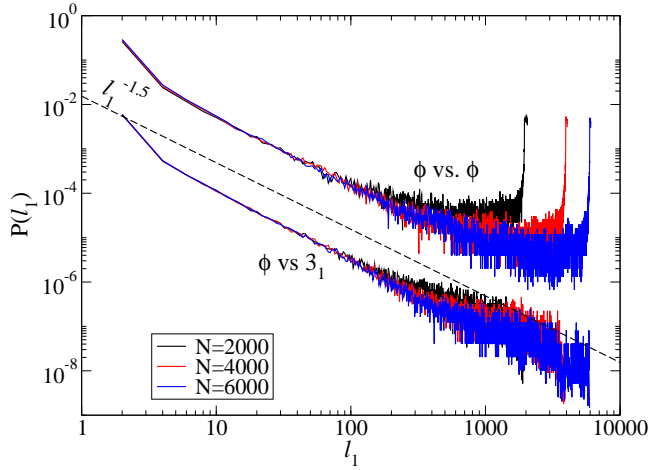


FIG. 3: Log-log plots of $P(l_1)$ for \emptyset vs \emptyset (upper curves, for three values of N), and \emptyset vs 3_1 (lower curves, shifted one decade down). The dashed line represents a power-law $l_1^{-1.5}$. Each N includes the statistics in the interval $[N - 50, N + 50]$: this does not alter the power-law tail and increases the statistics considerably.

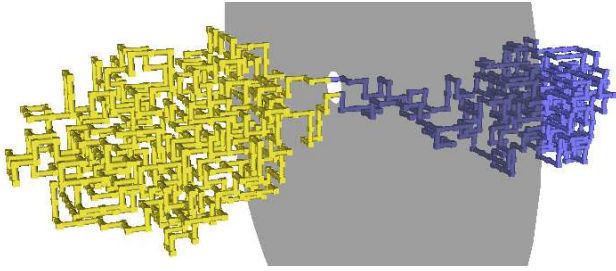


FIG. 4: Example of a wall-globule system. The hole (white) separates the $N = 1000$ chain into two globuli with 3_1 knot (colored differently).

In this case the loop with the 3_1 knot obtains on average a fraction of the chain length equal to $3/7 \approx 0.43$, while $4/7 \approx 0.56$ go to the loop with 4_1 knot. This is evidenced in Fig. 2d by the linear fits of the average loop lengths as a function of N .

The law in Eq.(2) highlights the key role played by the topological invariant n_c in the delocalized regime. This role is further emphasized by considering the competition of two knots that are different but with the same n_c . Fig. 2e and 2f show the results for $3_1 \# 3_1$ vs 6_1 . We see that, while the fluctuations remain very broad, also in this case the $\langle l_i \rangle_N$'s still obey Eq. (2). In addition the shape of the histograms is quite symmetric as in the 3_1 vs 3_1 case. However, the possible convergence towards a flat histogram is definitely slower than in that case. These results suggest that the number of prime components of a knot is not a relevant invariant, unlike in the swollen regime.

In experiments the slipping link could be, e.g., a short (unknotted) ring which is not linked to the knotted one,

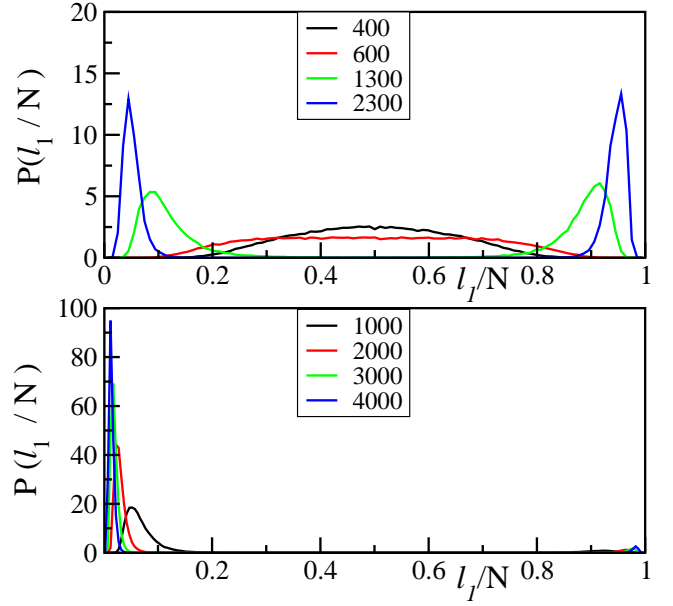


FIG. 5: Histograms of $P(l_1/N)$ for $3_1 \# 3_1$ (loop 1) vs 6_1 (top panel) and for 3_1 (loop 1) vs 4_1 (bottom panel) when the two globular loops are separated by an impenetrable wall. Different curves correspond to different N values.

but just constrains it to pass through its interior. To discover further consequences the topology may have in the globular phase we replace the slipping link by a sufficiently narrow hole in an impenetrable wall, Fig. 4. This schematizes the translocation of a ring polymer through a membrane or solid state nanopore, a phenomenon that, thanks to recent progress in nanotechnology can be investigated experimentally [15, 16]. A related biological issue is the effect that knots may have on the ejection process of packed viral DNA into the host cell [17, 18]. Due to the presence of the wall the two loops do not interact anymore and can be considered as two independent, knotted globuli in competition. As shown in Fig. 5 for a case with two different knots having however the same $n_{c1} = n_{c2} = 6$, $P(l_1/N)$ develops two remarkably symmetric peaks for $N \gtrsim 1000$, which become separated by a very high free energy barrier already at $N \approx 2300$, the maximum N for which our multiple chain sampling works efficiently. Similar results are obtained for the simpler case 3_1 vs 3_1 .

The situation turns out to be totally different when $n_{c1} \neq n_{c2}$. In these cases we observe an asymmetry, indicating a clear dominance of the globular loop hosting the knot with higher n_c . This dominance becomes more and more pronounced as N increases. We report the results for the case 3_1 vs 4_1 with rings of length up to $N = 4000$ in Fig.5.

How topology can produce the asymmetry manifested by the above results for the wall case can be explained as

follows. The equilibrium share of the ring length between the two globuli should stably minimize the free energy. Due to independence, the total free energy is simply the sum of the free energies of the two globuli. We can assume that in the relevant ranges explored by our simulations both l_1 and l_2 are sufficiently large for Eq.(2) to give a reasonable approximation of the globule free energy. The surface term in F_N , if taken into account as the only correction, implies that both configurations in which one of the globuli has length $\lesssim N$, while the other is close to minimal, realize equivalent stable minima of the total free energy with constraint $l_1 + l_2 = N$. Let us indicate by m_1 and m_2 the value of l_1 and l_2 , respectively, in the stable configuration in which it happens to be the shorter loop. From Eq.(2) one gets for the ratio of canonical probabilities of these configurations:

$$\ln \left(\frac{P(l_1 = N - m_2, l_2 = m_2)}{P(l_1 = m_1, l_2 = N - m_1)} \right) = \sigma \left[(N - m_2)^{2/3} + m_2^{2/3} - (N - m_1)^{2/3} - m_1^{2/3} \right] + (\alpha - 2) \ln \left(\frac{(N - m_2)m_2}{(N - m_1)m_1} \right) + C \left[\frac{n_{c1}^a}{N - m_2} + \frac{n_{c2}^a}{m_2} - \frac{n_{c1}^a}{m_1} - \frac{n_{c2}^a}{N - m_1} \right] \quad (3)$$

In the case $n_{c1} = n_{c2}$ the presence of the topological correction does not matter, and thus we expect to see with the same frequency a dominance of either one of the two globuli. The only topological effect left could be due to a slight difference between m_1 and m_2 in the cases in which the two knots in 1 and 2 are not identical. However, this difference should be extremely small. Indeed, for example the minimal lengths of lattice knots with the same n_c , which are lower bounds for m_1 and m_2 , are known to be almost coincident [19]. When we instead have $n_{c1} \neq n_{c2}$, the two configurations favored by surface tension are not equally probable anymore. The term apt to determine a substantial deviation of the quantity in Eq.(3) from zero originates in fact from the topological correction:

$$C \left[\frac{n_{c2}^a}{m_2} - \frac{n_{c1}^a}{m_1} \right] \quad (4)$$

The main reason for this deviation is the remarkably large absolute value of C , which amplifies any even slight difference $\frac{n_{c1}^a}{m_2} - \frac{n_{c2}^a}{m_1}$. To get an estimate of the quantity in Eq.(4) for the first knots, we calculated it for $C \approx -170$ and $a \simeq 1.45$, the values found for $T/J = 2.5$ [10], and m_1 and m_2 replaced by the existing estimates of the minimal lattice knot lengths [19], consistently with the peak structures reported in Fig.5. For the case 3_1 vs 4_1 , the value of (4) turns out to be ≈ 7.5 .

Thus, a topological mechanism explains why a stable configuration is that in which the globule with smaller n_c is reduced to a minimal size, while the other takes

most of the ring length. This novel phenomenon should be relevant, e.g., for a slow dynamics of translocation of globular knotted ring polymers through membrane pores.

Putting things in perspective, although necessarily limited to the less complex knots, our results are accurate enough to clearly qualify n_c as the invariant controlling delocalization in the globular phase and determining unexpected thermodynamic effects of genuinely topological nature. The outlined scenario is totally different from that expected in the swollen polymer regime. Even if unusually large chain lengths need to be explored in order to fully clarify their asymptotics, the discovered phenomena are most relevant in practice for finite N .

Acknowledgments

This work is supported by “Fondazione Cassa di Risparmio di Padova e Rovigo” within the 2008-2009 “Progetti di Eccellenza” program.

-
- [1] E. Orlandini, S. G. Whittington, Rev. Mod. Phys. **79**, 611 (2007).
 - [2] C. C. Adams, *The Knot Book* (Freeman, 1994).
 - [3] B. Marcone, E. Orlandini, A. L. Stella, F. Zonta, J. Phys. A: Math. Gen. **38**, L15 (2005).
 - [4] O. Farago, Y. Kantor, M. Kardar, Europhys. Lett. **60**, 53 (2002).
 - [5] M. Baiesi, E. Orlandini, and A. L. Stella, J. Stat. Mech. p. P06012 (2010).
 - [6] M. Baiesi, G. T. Barkema, and E. Carlon, Phys. Rev. E **81**, 061801 (2010).
 - [7] C. Vanderzande, *Lattice Models of Polymers* (Cambridge University Press, 1998).
 - [8] B. Marcone, E. Orlandini, A. L. Stella, F. Zonta, Phys. Rev. E **75**, 041105 (2007).
 - [9] P. Virnau, Y. Kantor, M. Kardar, J. Am. Chem. Soc. **127**, 15102 (2005).
 - [10] M. Baiesi, E. Orlandini, A. L. Stella, Phys. Rev. Lett. **99**, 058301 (2007).
 - [11] N. Madras and G. Slade, *The Self-Avoiding Walk* (Birkhäuser, 1993).
 - [12] A. L. Owczarek, T. Prellberg, R. Brak, Phys. Rev. Lett. **70**, 951 (1993).
 - [13] M. C. Tesi, E. J. Janse Van Rensburg, E. Orlandini, S. G. Whittington, J. Stat. Phys. **82**, 155 (1996).
 - [14] A. Y. Grosberg and A. R. Khokhlov, *Statistical physics of macromolecules*, AIP series in polymers and complex materials (American Institute of Physics, New York, 1994), ISBN 1-56396-071-0.
 - [15] J. J. Kasianowicz, E. Brandin, D. Branton, D. W. Deamer, Proc. Natl. Acad. Sci. USA **93**, 13770 (1996).
 - [16] R.M.M. Smeets, U. F. Keyser, D. Krapf, M. Y. Wu, N. H. Dekker, C. Dekker, Nano Lett. **6**, 89 (2006).
 - [17] D. Marenduzzo, E. Orlandini, A. Stasiak, d. W. Sumners, L. Tubiana, and C. Micheletti, Proc Natl Acad Sci U S A **106**, 22269 (2009).
 - [18] R. Matthews, A. A. Louis, J. M. Yeomans, Phys. Rev. Lett. **102**, 088101 (2009).
 - [19] E. J. Janse van Rensburg, S. D. Promislow, J. Knot Theory Ramif. **4**, 115 (1995).